Error mapping in DOFP Stokes images and its use for retardance calibration

Benjamin Le Teurnier, Matthieu Boffety, François Goudail

Error mapping in Division of Focal Plane (DoFP) Stokes images and its use for retardance calibration

B. Le Teurnier[1], M. Boffety[1], and F. Goudail[1]

[1]Laboratoire Charles Fabry, Institut d'Optique Graduate School, CNRS, Université Paris-Saclay 11, 91127 Palaiseau, France

ABSTRACT

Integrated Division of Focal plane (DoFP) cameras have recently been developed for polarimetric imaging. These sensors use a grid composed of four different pixels with four different polarizers engraved on them. Four of these different pixels form a superpixel which enables the estimation of the linear Stokes vector with a single acquisition. Estimation of the full Stokes vector can be done by adding a retarder in front of the DoFP camera and performing at least two acquisitions with two different angular positions of the retarder.

As a drawback, DoFP sensors are particularly sensitive to the spatial variations of the scene within a superpixel. Therefore, if these variations are non-negligible compared with the measurement noise, the estimation of the state of polarization is corrupted. We propose a method to map the superpixels in which the estimation can be trusted.

As an example of application, we demonstrate the benefit of using such a mapping to perform dynamic autocalibration of the retardance of the retarder placed in front of the camera for full Stokes imaging. Thanks to measurement redundancy, calibration of the retardance and estimation of the Stokes vector can be jointly performed provided three acquisitions for three different orientations of this retarder are made. However, this method may be perturbed by the spatial variations of a complex scene, and the proposed mapping enables to wisely choose the superpixels that are appropriate for calibration.

Keywords: Polarization, polarimetric imager

1. INTRODUCTION

Polarization imaging systems lead to contrasts that are invisible in conventional intensity images.[1–4] Such imaging system needs to acquire several analyses of the polarization in order to derive the polarimetric information. DoFP sensors enable to obtain these different analyses in a single acquisition. The existing DoFP are composed of four different pixels with different linear polarizers engraved on them. They allow the estimation of the linear polarization with a single acquisition and thus enable real time polarization imaging.[5–9] In order to measure the full Stokes vector, one can add a rotating retarder in front of this DoFP camera and perform at least two acquisitions for different orientations of the retarder.[10–13] With three acquisitions with a rotating retarder, the retardance can be calibrated alongside the estimation of the Stokes parameters.[11,14–16]

As a downside, with a DoFP sensor the different pixels used for the estimation of a Stokes vector are not localized at the same place and thus are not seeing the same part of the scene. Therefore, if the scene contains fast spatial variations there will be a strong difference between the polarization seen by each pixel and the estimation will be wrong.

Thus we describe here a method to detect whether or not the variations of the scene within a super-pixel are too important to lead to a reliable estimation. This method uses the redundant information within the measurements of the super-pixel and an estimation of the spatial variations of the intensity in the scene. By combining these two criteria one can obtain an error map which tells where the estimation is not reliable.[17] We then use this error map to help the calibration of a retarder.

2. METHODOLOGY

2.1 DoFP polarization sensor

DoFP sensors are composed of an array of "super-pixels". Each one contains four pixels with linear polarizers with four different angle at 0°, 45°, 90° and 135°. The four measurements obtained with a super-pixel enable the estimation of the linear Stokes vector. To estimate the full Stokes vector one can use a rotating retarder and perform at least two acquisitions with two different orientations of the retarder. With N_{acq} acquisitions, a super-pixel leads to $N_{\text{mes}} = 4 \times N_{\text{acq}}$ measurements. These measurements are gathered in the vector $\mathbf{I}$ and this acquisition is modeled as:

$$\mathbf{I} = \mathbb{W}\mathbf{S}, \tag{1}$$

where $\mathbf{S} = (S_0, S_1, S_2, S_3)^T$ is the incident Stokes vector. It is of length $K = 4$ in the general case, but if we only estimate the linear polarization then we consider only its first 3 component and its length is $K = 3$. $\mathbb{W}$ is a $N_{\text{mes}} \times K$ matrix called measurement matrix of the super-pixel and describes the acquisition process of the super-pixel. The incident Stokes vector is estimated with:

$$\hat{\mathbf{S}} = \mathbb{W}^{+}\mathbf{I}, \tag{2}$$

with $\hat{\mathbf{S}}$ the estimated Stokes vector and the superscript $^+$ denotes the Moore-Penrose pseudo-inverse. This estimation model considers a homogeneous incident polarization state on the super-pixel. Unfortunately, the different pixels of the super-pixel usually receive different incident polarizations due to the spatial variations of the scene. If this variations are greater than the measurement noise, it may lead to a significant bias on the estimation of the polarization. We describe here a method to detect the super-pixels which lead to such unreliable estimations.

2.2 Redundancy criterion

Within a super-pixel, the number of measurements used for the estimation of the Stokes vector is larger than the number of parameters to estimate. This leads to redundancy between these measurements. The light intensity incident on the super-pixel can be estimated with $S_{0\_a} = I_0 + I_{90}$ and $S_{0\_b} = I_{45} + I_{135}$. In the ideal case, with no noise and a constant incident Stokes vector on the super-pixel, $S_{0\_a} = S_{0\_b}$. But if there is inconsistency between the measurements, we may have: $R_{lin} = I_0 + I_{90} - (I_{45} + I_{135}) \neq 0$. This criterion provides a quantitative evaluation of the inconsistencies between the measurements acquired by the super-pixel. But it does not take into account the calibration of the sensor and it is not applicable to imaging systems composed of a sensor and a rotating retarder used to measure the full Stokes vector.

We thus propose a generalization of this criterion. Using the singular value decomposition (SVD) of the measurement matrix $\mathbb{W}$, one has:

$$\mathbb{W} = \mathbb{U}\mathbb{D}\mathbb{V}^T, \tag{3}$$

where $\mathbb{U}$ and $\mathbb{V}$ are unitary matrices of dimensions $N_{\text{mes}} \times N_{\text{mes}}$ and $K \times K$. $\mathbb{D}$ is a $N_{\text{mes}} \times K$ matrix with a $K \times K$ first block which is diagonal and contains the singular values of the measurement matrix $\mathbb{W}$. The last $N_{\text{mes}} - K$ rows of $\mathbb{D}$ contains only zeros. The superscript ^{T} denotes the transposition. By substituting Eq. 3 in Eq. (2) we have:

$$\mathbb{U}^T\mathbf{I} = \mathbb{D}\mathbb{V}^T\mathbf{S}. \tag{4}$$

The last $N_{\text{mes}} - K$ elements of the vector $\mathbb{U}^T\mathbf{I}$ are null, due to the properties of $\mathbb{D}$, in the ideal case when considering a homogeneous incident Stokes vector and in absence of noise. We then define the matrix $\mathbb{U}_R$ composed of the last $N_{\text{mes}} - K$ columns of the matrix $\mathbb{U}$ and compute:

$$\mathbf{R} = \mathbb{U}_R^T\mathbf{I}. \tag{5}$$

The vector $\mathbf{R}$ is null in the ideal case with a homogeneous incident Stokes vector and without noise. Furthermore, in this conditions and in the case of the sensor used alone for linear polarization estimation, the criterion $\mathbf{R}$ is a scalar and is proportional to R_{lin}.

In practice, we mostly have Poisson noise, but with a mean value high enough to consider it as an additive Gaussian random variable which variance is equal to the mean value of the signal. We can derive from this

consideration that the elements of the vector $\mathbf{R}$ are centered Gaussian random variables. One can thus obtain a vector of standard Gaussian random variable $\mathbf{T}$ whose elements are defined with:

$$\mathbf{T}(i) = \frac{\mathbf{R}(i)}{\sqrt{\mathrm{VAR}[\mathbf{R}(i)]}}. \tag{6}$$

Then, if the noise is the only perturbation affecting the measurements, the Euclidean norm of the vector $\mathbf{T}$ follows a χ^2 law and a threshold can be applied with a constant false alarm rate.[17] This criterion based on the redundant information is then able to detect whether the inconsistencies between the measurements are significant in front of the noise.

This detector suffers a flaw. It does not detect the intensity variations within the super-pixel. This is highlighted on Figure 1 where are displayed the estimated intensity S_0 with the detected inconsistencies displayed in red and the estimated degree of linear polarization (DoLP). The scene acquired is a blank cardboard with large black letters printed on it. We used the DoFP sensor alone to estimate only the linear polarization state. We observe, on the estimated DoLP, estimation artifacts located on the intensity edges of the scene: estimated DoLP is significantly higher on these edges without physical explanation. However the detector defined in Equation (6) does not detect these edges as problematic even though there is clearly an error of estimation. Thus, we need to use a separate intensity variation detector to help this redundancy based criterion.

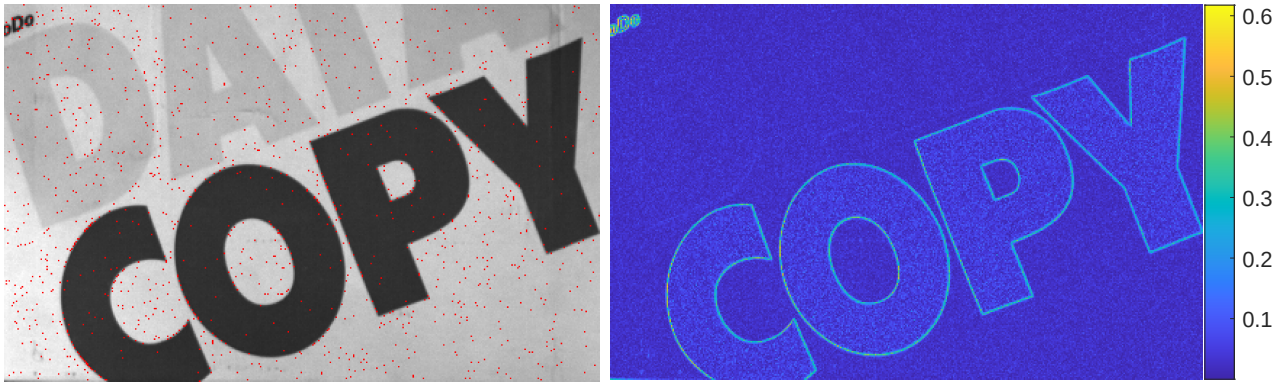

Figure 1. An example of error map and estimated DoLP on a scene composed of a blank cardboard with large black letters printed on it. The intensity estimated in gray level with the error map displayed in red (left) and the estimated DoLP (right). The error map used here uses only the redundancy criterion to detect the inconsistencies between the measurements within a super-pixel.

2.3 Intensity Variation detection

We designed an intensity variation detector with constant false alarm rate. Doing so, we only need to set one parameter, the false alarm rate, to apply thresholds to both the redundancy based criterion and the intensity variation criterion.

This intensity variation detector uses the intensity estimations on neighboring super-pixels, as shown Figure 2, so that it is independent from the polarization states. This detector uses the log-likelihood ratio between the two following hypotheses:

- There is no intensity variation and the signal is mostly Poisson noise of constant mean over the super-pixels.
- There is an intensity variation within this array and we consider four regions within the 4×4 pixels array selected. The signal within the four regions follows four different Poisson laws of parameters λ_a, λ_b, λ_c and λ_d as shown on Figure 2.

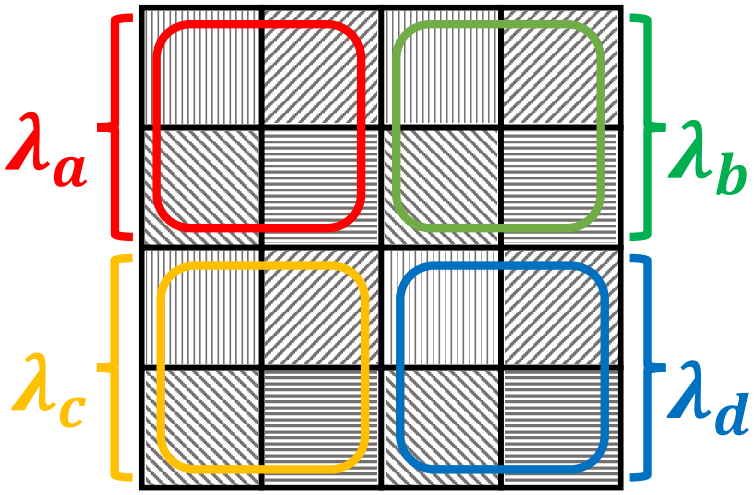

Figure 2. A 4×4 pixels array. The four pixels at the center form the super-pixel of interest. The four super-pixels highlighted by the color squares are used to measure the four parameters λ_a, λ_b, λ_c and λ_d corresponding to the sum of the measured intensities within these super-pixels.

Then the log-likelihood ratio can be computed as:[17]

$$\ln(\mathcal{R}) = 4\left[\frac{1}{4}\sum_k(\hat{\lambda}_k \ln(\hat{\lambda}_k)) - \frac{\sum_k \hat{\lambda}_k}{4}\ln\left(\frac{\sum_k \hat{\lambda}_k}{4}\right)\right]. \tag{7}$$

where the $\hat{\lambda}_k$ are the estimation of the parameters λ_k for the four different super-pixels surrounding the super-pixel of interest. We demonstrated[17] that this log-likelihood ratio is proportional to a χ^2 law when the measurement noise is the only perturbation. Thus a threshold can be applied with a constant false alarm rate to detect an intensity variation.

The error map obtained with this intensity variation detector is then combined with the error map based on the redundancy based criterion. An example is shown on Figure 3 where we use the same cardboard scene as for 1. In green is displayed the error map obtained with the redundancy criterion and in red the error map given by the intensity variation detector for a false alarm rate $P_{\text{fa}} = 10^{-3}$. In yellow we display the pixels for which both criteria detect anomalies. As we can see the intensity variation detector detects well the edges of the black letters where we observed estimation artifacts. Thus it is a good complement to the redundancy based criterion.

3. APPLICATION

We demonstrate the utility of such error map for the dynamic calibration of a retarder placed in front of the DoFP camera for the estimation of the full Stokes vector. Such calibration is possible when at least three acquisitions are performed for different orientations of the retarder.

3.1 Autocalibration

Dynamic calibration (we usually call it autocalibration) is performed by jointly estimating the retardance δ of the retarder and the Stokes vector $\mathbf{S}$ from the measurements of a super-pixel by using the redundancy between the intensity measurements within a super-pixel. To do so, we optimize the criterion $\mathcal{F}(\delta)$:

$$\hat{\delta} = \arg\min_{\delta}[\mathcal{F}(\delta)], \tag{8}$$

with

$$\mathcal{F}(\delta) = \left\|[\mathbb{I}_d - \mathbb{W}(\delta)\mathbb{W}(\delta)^+]\mathbf{I}\right\|^2, \tag{9}$$

Figure 3. The error map obtained by combining the redundancy criterion and the intensity variation detector. The intensity is displayed in gray level, the redundancy criterion based detector in green and the intensity variation detection in red. In yellow appear the pixels detected by both detectors as problematic.

where $\mathbf{I}$ is the vector of the measured intensities, $\mathbb{I}_d$ the identity matrix and $\mathbb{W}(\delta)$ the measurement matrix of the super-pixel considering the several acquisitions for the several orientations of the retarder of retardance δ.[16] Then the estimated retardance $\hat{\delta}$ is introduced in the measurement matrix $\mathbb{W}(\delta)$ which is substituted in Equation 2:

$$\hat{\mathbf{S}} = \mathbb{W}(\delta)^{+}\mathbf{I}, \tag{10}$$

Only one super-pixel is needed to perform this autocalibration. However, using a set of several super-pixels reduces the uncertainty on this estimation. In order to wisely choose the super-pixels used for this autocalibration, it has been shown[16] that, in the presence of additive Gaussian noise, we must consider the super-pixels which maximize the value of the reduced signal to noise ratio $\mathrm{SNR}_\delta = \mathrm{SNR} \times \mathrm{DoLP}$. Furthermore, there is the constraint that $\mathrm{SNR}_\delta > 8$, otherwise the autocalibration is not possible. In practice we thus choose the super-pixels which maximize the estimated $\hat{\mathrm{SNR}}_\delta$ and respect $\hat{\mathrm{SNR}}_\delta > 8$.

3.1.1 Error mapping

However as seen on Figure 1, it often happens that the estimated DoLP, and then $\hat{\mathrm{SNR}}_\delta$, is over estimated due to artifacts of estimation where there is significant spatial variations in the scene. This may lead to select super-pixels for the autocalibration which are not reliable. This scenario is shown on Figure 4 where are displayed the intensity image of the scene used with the set of super-pixels selected by maximizing the estimated $\hat{\mathrm{SNR}}_\delta$ displayed in red (left), and the histogram of the estimated retardances for this set of super-pixels plotted in red (right). We are using a quarter wave-plate (QWP) so we expect a retardance close to 90°. The super-pixels selected are mainly located on intensity edges for which we have seen that the estimated DoLP is biased. These super-pixels lead to huge errors on the estimated retardances which are not gathered around the expected value.

Then we compute the error map for this scene which is displayed on Figure 5 in yellow on the gray level intensity image. Then we use this error map to select the super-pixels which maximize the value of $\hat{\mathrm{SNR}}_\delta$ outside of the set of super-pixels which have been detected as unreliable. This lead to the set of super-pixels displayed in green on Figure 4 (left). They are located mostly on a smooth area of the scene where the estimation is more reliable. The histogram of the values of estimated retardances using this set of super-pixels is plotted in green (right). We see that this histogram is centered around the expected value for the retardance with a mean value of 87.6° and a standard deviation of 4.6°. This set of super-pixels thus gives a suitable estimation of the retardance for the used wave-plate (90°).

4. CONCLUSION

In conclusion, the generalized redundancy criterion $\mathbf{R}$ provides information about the inconsistencies between the measurements within a super-pixel and can take into account the calibration of the sensor as well as being able to work with full Stokes imaging system. We derived a CFAR detector from this criterion and as it is

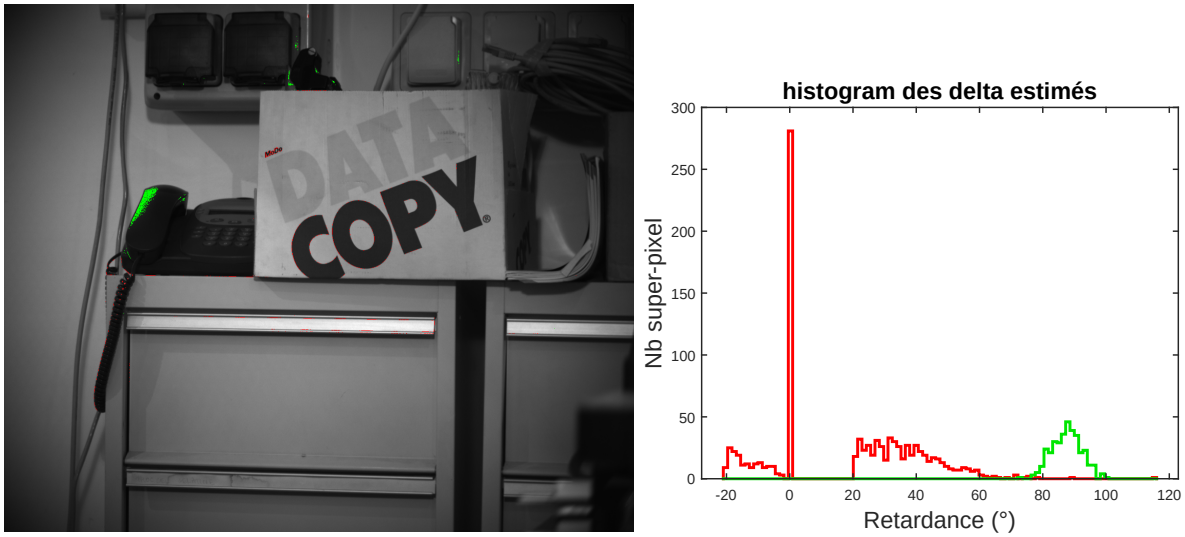

Figure 4. The histogram of the estimated retardance value for the N chosen super-pixels. Without using the error map (in red) and with excluding the pixels detected by the error map (in green)

Figure 5. The error map which combine the two criteria based respectively on the redundant information and on the variation of intensity. It is displayed in yellow on the gray level image of intensity.

not able to detect errors which are due to intensity edges we proposed another CFAR detector to detect these intensity variations. The error map obtained by combining these two detectors enables to have a map of the super-pixels for which we can not trust the estimation. We demonstrated that such mapping makes it possible to perform dynamic calibration of the retardance of a wave-plate used within a full Stokes imaging system even with a complex scene. Such error mapping may be useful for other applications such as demosaicing strategies.

REFERENCES

[1] Tyo, J. S., Goldstein, D. L., Chenault, D. B., and Shaw, J. A., "Review of passive imaging polarimetry for remote sensing applications," *Applied Optics* **45**, 5453 (aug 2006).

[2] Thilak, V., Voelz, D. G., and Creusere, C. D., "Polarization-based index of refraction and reflection angle estimation for remote sensing applications," *Applied Optics* **46**, 7527 (oct 2007).

[3] Foldyna, M., Martino, A. D., Ossikovski, R., Garcia-Caurel, E., and Licitra, C., "Characterization of grating structures by mueller polarimetry in presence of strong depolarization due to finite spot size," *Optics Communications* **282**, 735–741 (mar 2009).

[4] Mu, T., Bao, D., Han, F., Sun, Y., Chen, Z., Tang, Q., and Zhang, C., "Optimized design, calibration, and validation of an achromatic snapshot full-stokes imaging polarimeter," *Optics Express* **27**, 23009 (jul 2019).

[5] Powell, S. B. and Gruev, V., "Calibration methods for division-of-focal-plane polarimeters," *Optics Express* **21**, 21039 (aug 2013).

[6] Chen, Z., Wang, X., and Liang, R., "Calibration method of microgrid polarimeters with image interpolation," *Applied Optics* **54**, 995 (feb 2015).

[7] Feng, B., Shi, Z., Liu, H., Liu, L., Zhao, Y., and Zhang, J., "Polarized-pixel performance model for DoFP polarimeter," *Journal of Optics* **20**, 065703 (may 2018).

[8] Roussel, S., Boffety, M., and Goudail, F., "Polarimetric precision of micropolarizer grid-based camera in the presence of additive and poisson shot noise," *Optics Express* **26**, 29968 (oct 2018).

[9] Lane, C., Rode, D., and Rösgen, T., "Calibration of a polarization image sensor and investigation of influencing factors," *Applied Optics* **61**, C37 (oct 2021).

[10] Qi, J., He, C., and Elson, D. S., "Real time complete stokes polarimetric imager based on a linear polarizer array camera for tissue polarimetric imaging," *Biomedical Optics Express* **8**, 4933 (oct 2017).

[11] Shibata, S., Hagen, N., and Otani, Y., "Robust full stokes imaging polarimeter with dynamic calibration," *Optics Letters* **44**, 891 (feb 2019).

[12] Roussel, S., Boffety, M., and Goudail, F., "On the optimal ways to perform full stokes measurements with a linear division-of-focal-plane polarimetric imager and a retarder," *Optics Letters* **44**, 2927 (may 2019).

[13] Li, X., Teurnier, B. L., Boffety, M., Liu, T., Hu, H., and Goudail, F., "Theory of autocalibration feasibility and precision in full stokes polarization imagers," *Optics Express* **28**, 15268 (may 2020).

[14] Goudail, F., Li, X., Boffety, M., Roussel, S., Liu, T., and Hu, H., "Precision of retardance autocalibration in full-stokes division-of-focal-plane imaging polarimeters," *Optics Letters* **44**, 5410 (nov 2019).

[15] Li, X., Hu, H., Goudail, F., and Liu, T., "Fundamental precision limits of full stokes polarimeters based on DoFP polarization cameras for an arbitrary number of acquisitions," *Optics Express* **27**, 31261 (oct 2019).

[16] Le Teurnier, B., Li, X., Boffety, M., Hu, H., and Goudail, F., "When is retardance autocalibration of microgrid-based full stokes imagers possible and useful?," *Optics Letters* **45**, 3474 (jun 2020).

[17] Le Teurnier, B., Li, N., Boffety, M., and Goudail, F., "Definition of an error map for DOFP polarimetric images and its application to retardance calibration," *Optics Express* (feb 2022).